Strong absorption radii from reaction cross section measurements for neutron-rich nuclei

N. Aissaoui,[1] N. Added,[1] N. Carlin,[1] G. M. Crawley,[2,3] S. Danczyk,[2] J. Finck,[4] M. M. de Moura,[1] D. Hirata,[5] D. J. Morrissey,[2,6] S. J. Sanders,[7] J. Stasko,[2] M. Steiner,[2] A. A. P. Suaide,[1] E. M. Szanto,[1] A. Szanto de Toledo,[1] M. Thoennessen,[2,3] and J. A. Winger[8]

[1]*Departamento de Física Nuclear, Instituto de Física, Universidade de São Paulo,*
Caixa Postal 66318, 05315-970 São Paulo, São Paulo, Brazil
[2]*National Superconducting Cyclotron Laboratory, Michigan State University, East Lansing, Michigan 48824*
[3]*Department of Physics and Astronomy, Michigan State University, East Lansing, Michigan 48824*
[4]*Department of Physics, Central Michigan University, Mt. Pleasant, Michigan 48859*
[5]*Japan Synchrotron Radiation Research Institute (JASRI), Spring-8, Kamigori, Hyogo 678-12, Japan*
[6]*Department of Chemistry, Michigan State University, East Lansing, Michigan 48824*
[7]*Department of Physics and Astronomy, University of Kansas, Lawrence, Kansas 66045*
[8]*Department of Physics and Astronomy, Mississippi State University, Mississippi 39762*

Energy-integrated reaction cross sections have been measured at energies ranging from 38 to 80 MeV/nucleon for various exotic neutron-rich isotopes of Al, Si, P, S, Cl, Ar, K, Ca, Sc, and Ti stopping in Si. An experimental technique is employed where Si detectors are used for both particle identification and to serve as the target material. The reduced strong absorption radii r_0^2 are deduced and compared with other experimental results. The radius dependence on the neutron number was studied and a trend of increasing reduced radius with neutron excess was found. This behavior is similar to that seen in lighter systems, although less pronounced than found there. The implications of this result on the conjectured existence of neutron halo or skin nuclei is discussed. [S0556-2813(99)03609-2]

PACS number(s): 25.60.Dz, 24.10.Ht, 27.30.+t, 27.40.+z

I. INTRODUCTION

The availability of beams of radioactive nuclei has provided the nuclear physics community with a powerful tool to study the structure of nuclei far from stability. A considerable amount of both experimental and theoretical work has been devoted to this subject [1–10]. In particular, nuclear matter radii and density distributions have been studied through measurements of total reaction cross sections. The knowledge of these radii is of fundamental interest since any deviations observed from the expected $A^{1/3}$ dependence with nuclear mass in the case of neutron- or proton-rich nuclei can be taken to suggest nuclear structure effects. The observation of unusually large interaction radii for ^{11}Li and ^{14}Be has been attributed to just such structure effects corresponding to the spatial distribution of the nucleons inside the nucleus. In particular, these nuclei are thought to have a neutron halo [1,4]. More generally, Mittig *et al.* [7] have reported a surprising linear dependence of the reduced strong absorption radius on the neutron-excess. This trend has been confirmed for lighter nuclei [9], whereas the comparable behavior for heavier nuclei is less pronounced [9,10].

At higher energies, typically between 400*A* and 900*A* MeV, interaction cross section measurements have been used to probe the radial extent of matter densities of exotic nuclei. In particular, the separability of the interaction radii into two components has been verified both experimentally [1] and theoretically using the Glauber model [14,15]. This separability is operationally expressed by an interaction cross section that is related to the radii as $\sigma_I = \pi[R_I(p) + R_I(t)]^2$, where $R_I(p)$ and $R_I(t)$ are the nuclear interaction radii of the projectile and the target nuclei, respectively. The interaction cross section σ_I is defined as the total cross section leading to a change of the nucleon number in the incident nucleus, which is usually obtained by a transmission technique [1]. At intermediate energies, ranging from 10*A* to 100*A* MeV, the measurement of σ_I is typically performed using the associated-γ method [7,8]. However, this technique suffers a limitation by underestimating the reaction cross section in the case of reactions induced by neutron-rich nuclei where the contribution of breakup reactions that leave the final nuclei in the ground state or at very low excitation energy become significant. To overcome these difficulties, a direct method has been proposed by Villari *et al.* [9] which permits strong absorption radii to be obtained from reaction cross section measurements. Making use of a similar technique, we have recently performed reaction cross section measurements on *f-p* shell exotic neutron-rich nuclei and extracted the strong absorption radii [10], thus extending the available experimental data. The present work has two principal objectives. The first is to extend the systematics of strong absorption radii based on reaction cross sections in order to investigate the dependence of these radii on isospin. The second is to verify *a posteriori* the reliability of the parametrization which is commonly used to deduce the strong absorption radii by performing measurements at different primary-beam energies than used in the earlier measurements.

The paper is organized as follows. After a description of the experimental technique in Sec. II, the experimental data are presented in Sec. III. These data are discussed in Sec. IV. A summary of the results and conclusions are presented in Sec. V.
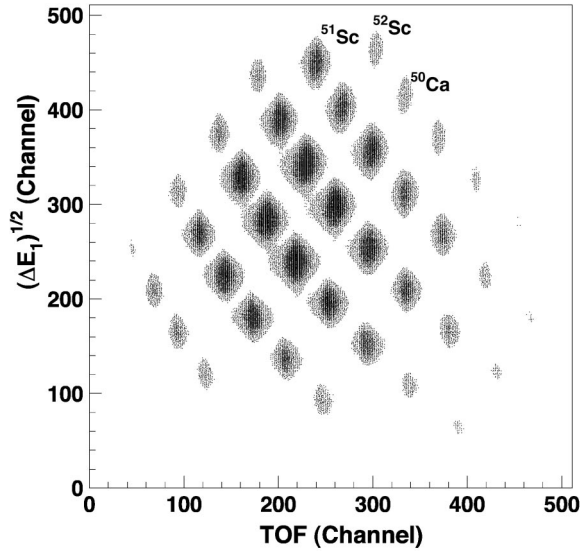
FIG. 1. Identification matrix ($\sqrt{\Delta E_1}$ vs TOF) obtained with the 90*A* MeV ^{55}Mn primary beam.

II. EXPERIMENTAL PROCEDURE

The experiment presented in this work was performed at the National Superconducting Cyclotron Laboratory (NSCL) at Michigan State University. The experimental details are similar to those used in our earlier work [10]. The secondary radioactive beams were produced through the projectile fragmentation of a 50*A* MeV (90*A* MeV) ^{55}Mn primary beam on a 103 mg/cm^2 (202 mg/cm^2) ^{9}Be target, situated at the target position of the A1200 mass separator. Two position sensitive (X and Y) parallel plate avalanche counters (PPAC's), located at the image points of the A1200, were utilized as beam monitors and provided position and angle measurements. These measurements also determined the trajectory of the observed particles for use in the time of flight analysis. The PPAC data were also used in the off-line analysis to reject those ions resulting from secondary scattering. The detection system is based on the combination of a stack of silicon detectors and a near-4π γ detector array. The stack was composed of five Si detectors of 75, 500, 500, 500, and 5000 μm thickness. The choice of this total thickness was dictated by the criterion of stopping completely all particles of interest ($Z>12$) with energies up to 90*A* MeV. For energy calibration purposes, low intensity 50*A* and 90*A* MeV ^{55}Mn beams were sent directly to the scattering chamber (no production target).

The silicon stack was surrounded by an array of seven hexagonal BaF$_2$ γ-ray detectors with close to 4π solid angle coverage. Each detector was 25 cm in length. The largest dimension of the front face was 6.5 cm. Six detectors were arranged longitudinally around the Si stack while the seventh was placed behind it. The identification of incident particles was done unambiguously by the energy loss in the first Si detector (ΔE_1) and by the trajectory corrected time of flight (TOF) between a scintillator detector, located approximately 40 m upstream to the target/detector, and the first Si detector. A two-dimensional identification spectrum $\sqrt{\Delta E_1} \times$ TOF, ob-

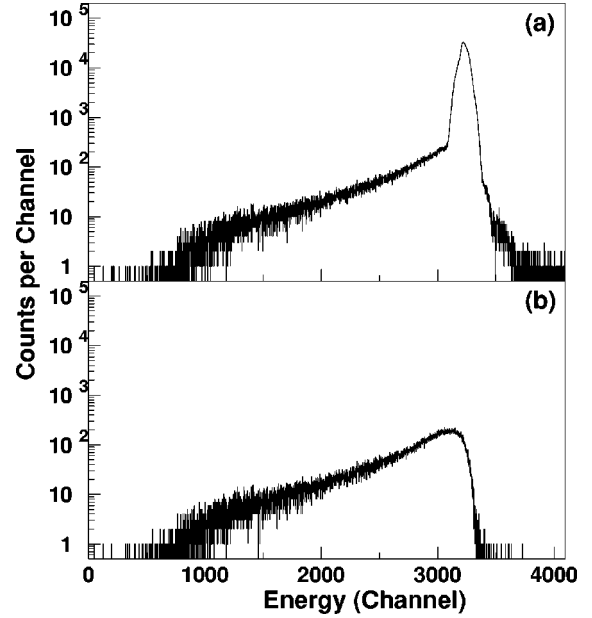FIG. 2. Typical total energy spectra for the ^{46}K isotope as obtained with the 90*A* MeV ^{55}Mn primary beam, (a) unconditioned spectrum, (b) coincidence spectrum with the 4π-γ array. The total energy was obtained by the sum of the energy losses in all Si detectors.

tained at a 90*A* MeV primary beam-energy, is shown in Fig. 1. Among the various observed and identified isotopes ^{51}Sc, ^{52}Sc, and ^{50}Ca are indicated in this figure.

III. RESULTS

The quantity measured with the technique described above is the mean energy-integrated reaction cross section $\bar{\sigma}_R$ which is given by the expression

$$\bar{\sigma}_R = \frac{\int_0^{E_{max}} \sigma_R(E)(dR/dE)dE}{\int_0^{R_{max}} dR}$$

$$= -\frac{m \ln(1-P_R)}{N_A R_{max}}, \tag{1}$$

where $m=28$ is the molecular weight of Si, N_A is Avogadro's number, and R_{max} the range of the incident particles. The Ziegler tables [11] were used to calculate R_{max} with an associated uncertainty of about 5%. The quantity P_R is the reaction probability which is calculated for each isotope by taking the ratio of the number of reaction events observed in the gated total energy spectrum and the total number of events in the corresponding ungated one. Typical energy spectra are shown in Fig. 2. In the evaluation of P_R, detection probability corrections for the γ rays were taken into account. This was achieved by evaluating the ratio, channel by channel, of the spectra corresponding to gated

and ungated events and excluding the quasielastic events. An average and constant detection probability of $80 \pm 3\%$ was found.

The trends of σ_R in the energies under consideration in this work are well accounted for by the predictions of a simple microscopic model based on individual nucleon-nucleon collisions. Within this framework, Kox *et al.* [12,13] proposed a semiempirical parametrization of σ_R which reproduces well most of the experimental data at the intermediate and high energy domains, using only one free parameter related to the surface transparency. Under this prescription, the parameter to be extracted from the experimental data is the reduced strong absorption radius r_0, defined as follows:

$$\sigma_R(E) = \pi r_0^2 f(E), \qquad (2)$$

where $f(E)$ is given by

$$f(E) = \left(A_p^{1/3} + A_t^{1/3} + a \frac{A_p^{1/3} A_t^{1/3}}{A_p^{1/3} + A_t^{1/3}} - C(E) \right)^2$$

$$\times \left(1 - \frac{V_B}{E_{c.m.}} \right), \qquad (3)$$

$$C(E) = 0.31 + 0.014 E/A, \qquad (4)$$

where A_p and A_t are the projectile and target mass numbers, $a = 1.85$ is a mass asymmetry parameter which is related to the volume overlap of the projectile and target, $C(E)$ is an energy dependent transparency, and V_B is the Coulomb barrier.

From Eqs. (1)–(4), the experimental reaction cross sections and the square of the strong absorption radii were calculated. The results obtained for all of the studied isotopes at both primary beam energies are presented in Tables I and II. In Fig. 3, the values obtained for r_0^2 are plotted as a function of the mass number for the Si, P, S, Cl, Ar, K, Ca, Sc isotopes. We included in the plots the results obtained in the present work at primary beam energies of $50A$ and $90A$ MeV along with those obtained in the previous work at $70A$ MeV [10]. The large error bars observed for a few points are due to the low statistics associated with masses lying at extremes of the identification spectrum. This spectrum was optimized for a given magnetic field setting for masses in the middle. In general these is good agreement among the measurement at the different energies. There is an exception, however, for the ^{41}Ar isotope, where the experimental radius was found in the previous work [10] to be unexpectedly high despite a small experimental uncertainty. In the newer measurements we obtain a different value that is in better agreement with the systematics. Although there is no clear explanation for the discrepancy, it is possible that a systematic error was made in the former analysis in obtaining the efficiency correction for isotopes lying at the limits of the magnetic field conditions. The solid lines represent Glauber-type calculations to be discussed in the next section. The good agreement obtained for the r_0^2 values from the three different primary

TABLE I. The mean energy-integrated reaction cross section and associated radii for the various isotopes selected from the fragmentation at primary beam energy of $50A$ MeV. The quoted errors were obtained by considering the statistical errors and those associated to the range evaluation.

A	Z	E/A (MeV)	$\bar{\sigma}_R$ (mb)	$\delta\bar{\sigma}_R$ (mb)	r_0^2 (fm^2)	δr_0^2 (fm^2)
53	22	40.27	3344	257	1.544	0.118
54	22	39.67	3644	408	1.670	0.187
49	21	41.08	4095	491	1.940	0.233
50	21	40.57	3036	209	1.427	0.098
51	21	40.18	3081	208	1.436	0.097
52	21	39.51	2860	233	1.324	0.108
46	20	45.61	3433	422	1.645	0.202
47	20	43.24	2807	198	1.338	0.095
48	20	40.59	2826	180	1.342	0.085
49	20	40.04	2800	193	1.319	0.091
50	20	38.94	3024	339	1.415	0.159
44	19	45.16	2628	197	1.276	0.095
45	19	43.22	2551	162	1.230	0.078
46	19	41.00	2662	167	1.277	0.080
47	19	39.56	2721	204	1.297	0.097
48	19	38.16	3164	367	1.499	0.174
41	18	46.56	2427	215	1.204	0.107
42	18	44.48	2546	167	1.253	0.082
43	18	42.50	2510	157	1.227	0.076
44	18	40.58	2685	183	1.304	0.089
45	18	38.79	2886	252	1.393	0.122
39	17	45.82	2419	171	1.218	0.086
40	17	43.69	2414	151	1.206	0.076
41	17	41.65	2531	161	1.255	0.080
42	17	39.74	2497	179	1.230	0.088
36	16	46.17	2440	192	1.262	0.099
37	16	44.99	2260	143	1.157	0.073
38	16	42.83	2385	151	1.210	0.077
39	16	40.73	2466	167	1.242	0.084
34	15	45.91	2175	145	1.144	0.076
35	15	44.05	2246	140	1.170	0.073
36	15	41.89	2308	146	1.191	0.075
37	15	39.71	2551	195	1.306	0.099
32	14	44.78	2136	134	1.146	0.072
33	14	42.73	2151	131	1.141	0.070
34	14	40.81	2291	160	1.203	0.084
30	13	43.40	2047	124	1.121	0.068
31	13	41.47	2145	135	1.161	0.073
32	13	39.51	2400	166	1.285	0.089

beam energies supports the reliability of the semiempirical parametrization of Kox *et al.* [12,13] in the energy domain under consideration.

IV. DISCUSSION

As indicated above, a convenient way of representing the σ_R data is to express it in terms of the reduced strong absorption radius r_0 [see formula (2)] assuming that the energy

TABLE II. The mean energy-integrated reaction cross section and associated radii for the various isotopes selected from the fragmentation at primary beam energy of $90A$ MeV. The quoted errors were obtained by considering the statistical errors and those associated to the range evaluation.

A	Z	E/A (MeV)	$\bar{\sigma}_R$ (mb)	$\delta\bar{\sigma}_R$ (mb)	r_0^2 (fm^2)	δr_0^2 (fm^2)
50	21	73.46	3107	211	1.420	0.097
51	21	71.32	3076	176	1.393	0.080
52	21	69.43	3303	233	1.483	0.105
47	20	75.24	2856	186	1.334	0.087
48	20	72.81	2841	158	1.314	0.073
49	20	70.69	3003	173	1.376	0.079
50	20	68.84	3105	222	1.411	0.101
44	19	77.40	2758	190	1.320	0.091
45	19	74.59	2771	151	1.312	0.072
46	19	72.07	2849	153	1.335	0.071
47	19	69.91	2891	161	1.342	0.075
48	19	67.89	3073	225	1.413	0.103
41	18	79.91	2471	229	1.214	0.112
42	18	76.80	2631	150	1.277	0.073
43	18	73.89	2725	146	1.308	0.070
44	18	71.21	2778	150	1.319	0.071
45	18	68.89	2881	170	1.354	0.080
46	18	66.77	2893	237	1.347	0.110
39	17	79.12	2451	162	1.223	0.081
40	17	75.98	2596	142	1.280	0.070
41	17	72.99	2641	141	1.286	0.068
42	17	70.20	2747	151	1.323	0.073
43	17	67.72	2772	170	1.321	0.081
44	17	65.47	2828	275	1.334	0.130
37	16	78.09	2462	158	1.249	0.080
38	16	74.92	2503	139	1.253	0.069
39	16	71.85	2632	146	1.301	0.072
40	16	68.99	2639	154	1.290	0.075
41	16	66.39	2781	214	1.344	0.103
35	15	76.80	2324	160	1.199	0.082
36	15	73.56	2445	144	1.244	0.073
37	15	70.48	2496	145	1.254	0.073
38	15	67.57	2603	171	1.292	0.085
39	15	64.83	2677	233	1.313	0.114
33	14	75.24	2448	251	1.286	0.132
34	14	71.92	2374	159	1.229	0.082
35	14	68.81	2462	180	1.258	0.092
36	14	65.88	2480	212	1.250	0.107
32	13	69.99	2462	232	1.298	0.123
33	13	66.85	2376	198	1.235	0.103

FIG. 3. The reduced strong absorption radii r_0^2 as a function of the mass number for various isotopes measured in this work (full symbols). The data represented by open triangles are taken from Ref. [10]. The solid lines represent Glauber-type calculations as described in the text.

tributions, has been used in order to compare the experimental results to theoretical calculations.

In Glauber theory the reaction cross section for projectile P is written

$$\sigma_R(P) = 2\pi \int_0^\infty db\, b[1 - T_P(b)], \qquad (5)$$

where $T_P(b)$, the squared modulus of the Glauber S matrix, is the transparency of the collision at impact parameter b. In the static density limit the transparency function is expressed as

$$T_P(b) = \exp\left[-\bar{\sigma}_{NN} \int d^2\mathbf{s}\,\rho_P^{(z)}(|\mathbf{s}|)\rho_T^{(z)}(|\mathbf{b-s}|) \right], \qquad (6)$$

where $\bar{\sigma}_{NN}$ is the free nucleon-nucleon (NN) cross section, at the relevant energy, appropriate for the projectile and target with densities ρ_P and ρ_T, and the

$$\rho_i^{(z)}(b) = \int_{-\infty}^{\infty} dz\,\rho_i(\sqrt{b^2+z^2}) \qquad (7)$$

dependence of σ_R is well accounted for by the parametrization of Kox *et al.* [13]. In fact, however, the determination of the matter radii and density distributions of nuclei far from stability is not straightforward. Until now, model-dependent approaches have been used to establish a link between the density distributions and cross sections. In our case, the optical limit of the Glauber model [15], using the relativistic mean-field theory (RMF) [16] to determine the density dis-
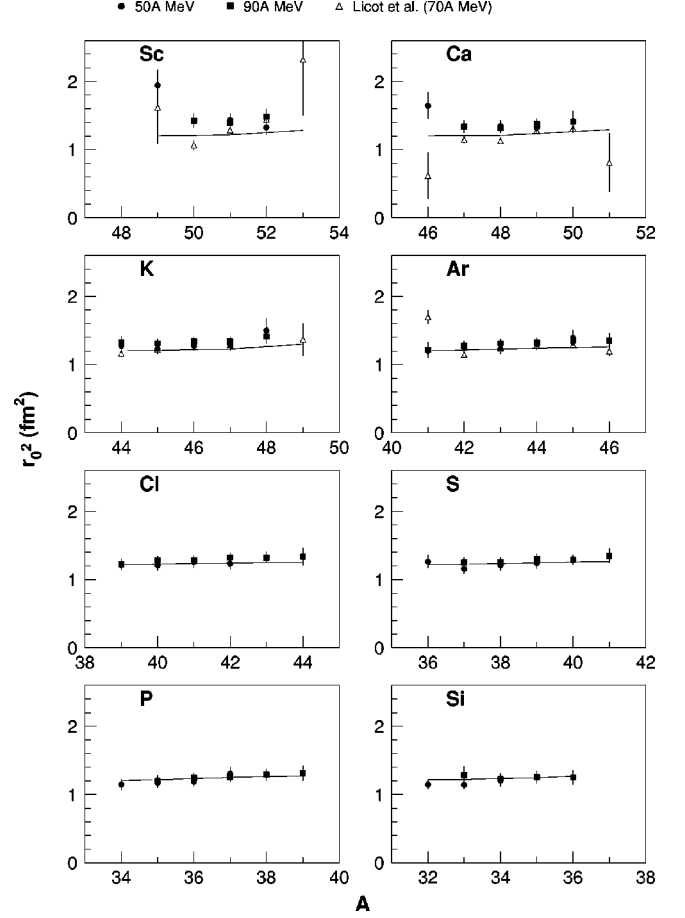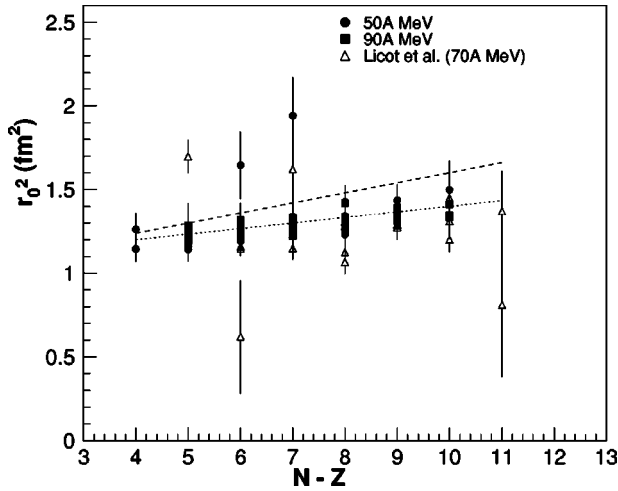
FIG. 4. Experimental r_0^2 values as a function of the neutron excess for all the isotopes studied in the present work at both primary beam-energies (full symbols). The data represented by open triangles are taken from Ref. [10]. The dotted line follow the parametrization relation $r_0^2 = (N-Z)/30 + 32/30$. The dashed line is the corresponding behavior observed in lighter systems.

are the z-integrated nucleon-density distributions.

The RMF theory is used to evaluate the projectile and target density distributions of Eq. (6). The RMF is a phenomenological many-body model, in which a spherical symmetry assumption is used in solving the self-consistent equations for nucleons and mesons interactions. Within this formalism, all of the essential information related to nuclear structure, such as masses, radii, single particle energy states, and wave functions (thus the density distributions) can be obtained from the effective Lagrangian containing the nuclear interaction. The TMA parameter set [17], which has been determined using experimental masses and charge radii over a wide mass range, from light to superheavy, is adopted for the calculations presented in this work. After the evaluation of the density distributions, the reaction cross section is obtained using Eq. (5). However, in order to compare the same quantities, the cross section is calculated for energies ranging from 10 MeV/nucleon (the value below which the reaction cross section was found to drop drastically [9]) to the incident energy in steps of 1 MeV/nucleon. A mean value of the reaction cross section $\bar{\sigma}_R$ is then deduced. This latter quantity is used to obtain the strong-absorption radii r_0^2 following the same parametrization presented in the previous section. The results of the calculations show a good agreement with the experimental results, as seen by the solid lines in Fig. 3. Indeed, the agreement is quite remarkable considering that these calculations are normally thought to be more suitable for higher energies (~ 400 MeV/nucleon) and that many known corrections, such as Coulomb deflection, Pauli blocking and Fermi motion effects, have not been included.

Looking at the dependence of the square of strong-absorption radii r_0^2 on the neutron excess $N-Z$, as displayed by Fig. 4, we find a global trend similar to that previously reported [9,10]. In particular, a slight linear increase of r_0^2 as
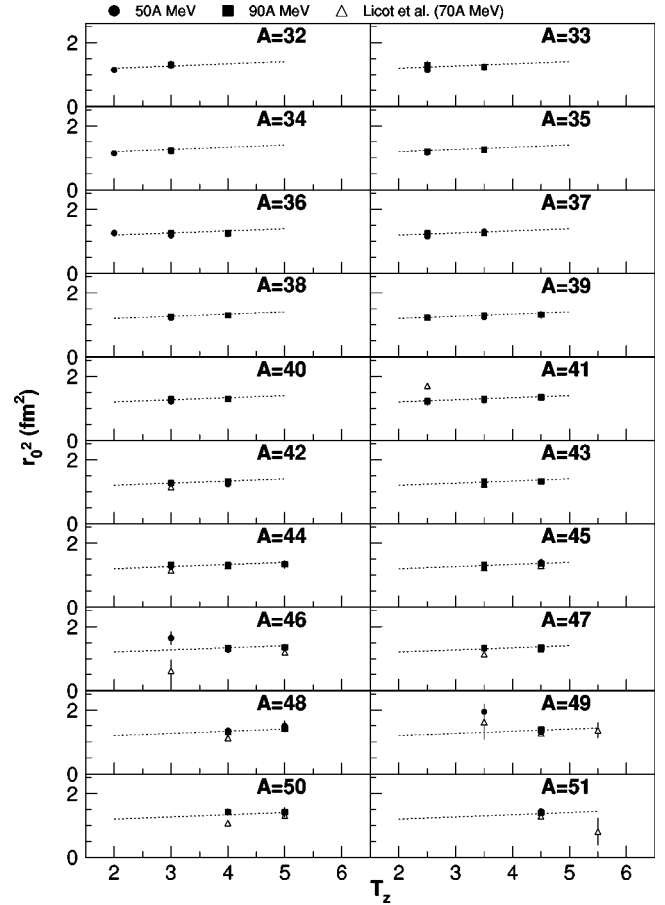

FIG. 5. Experimental r_0^2 values as a function of the isospin for all the isobars studied in the present work at both primary beam energies (full symbols). The data represented by open triangles are taken from Ref. [10]. All the dotted lines follow the equation $r_0^2 = T_z/15 + 32/30$.

a function of $N-Z$ is observed. As shown in the figure by the dotted lines, the average trend is successfully reproduced by the parametrization $r_0^2 = (N-Z)/30 + 32/30$ for $Z > 13$. This is somewhat different from the steeper linear dependence found for lighter nuclei [7] ($Z < 13$), for which the average trend follows a $r_0^2 = 0.06(N-Z) + 1$ dependence (dashed line in Fig. 4), but the qualitative agreement is preserved. It therefore appears that there are two different regimes where the dependence of the strong absorption radii on the neutron excess is dependent on the mass number (or atomic number). For each regime there is a dependence only on $N-Z$ and not directly on the atomic number. It should be noted that a nearly constant trend was suggested by Saint-Laurent *et al.* [8], where experimental considerations were then invoked to explain the observed discrepancies. In Fig. 5, we present the r_0^2 dependence on the isospin $T_z = (N-Z)/2$ for various measured isobars. It is interesting to note that the global parametrization deduced above still works in a satisfactory manner when applied separately for each isobar. The nuclear radii dependence on the isospin was studied both at intermediate and high energies for several light exotic nuclei [9,18,19]. The global trend found is an increase of the

strong-absorption radii r_0^2 with the isospin. This was corroborated by nonrelativistic Hartree-Fock calculations using a strong density-dependent Skyrme interaction [19] and by RMF calculations [5]. Our results are therefore in good agreement with these experimental results and theoretical predictions.

To explore the possible existence of neutron skin or halo structure, measured experimental cross sections at higher energies have been compared with Glauber-type calculations, using available isotope-shift data when possible, as has been done in Ref. [18] for $A = 17$ isobars. The observed differences between experimental and calculated values of the effective root-mean-square (rms) radii for large isospin is taken as evidence for a large tail component in the nuclear matter density. This tail component is missing in the model calculations. Such an analysis has been taken to suggest the presence of a neutron halo in ^{17}B. In a similar analysis proposed in Ref. [20] for Na isotopes, the increasing difference between ''neutron'' and ''proton'' radii, which were determined separately, was also attributed to the increase of the neutron skin. In the present work, considering the simple nature of our calculations, we can only expect to find supporting evidence for the existence or absence of neutron skin structures. In the previous work [10], based on the greater divergence between the experimental data and corresponding calculations with increasing neutron excess, the existence of small neutron skins has been proposed, in particular for the K and Sc isotopes. From the present results, as shown in Fig. 3, we have the same indications to support of the existence of neutron skins for the K isotopes and in a lesser degree for the Sc isotopes. In the latter case the somewhat moderated trends observed may suggest the existence of very thin neutron skins. For the other isotopes, no evidence of significant neutron skins is found.

V. SUMMARY AND CONCLUSIONS

In this work, reaction cross sections for a variety of exotic neutron-rich nuclei at intermediate bombarding energies have been measured. The reduced strong-absorption radii have been deduced for Al, Si, P, S, Cl, Ar, K. Ca, Sc, and Ti isotopes, using an appropriate parametrization. These data extend the previous systematics found for the strong-absorption radii. The obtained r_0^2 values from measurements at three different energies are in generally good agreement. These results have been compared to the predictions of Glauber-type calculations using RMF theory evaluated density distributions. Even though these calculations are generally considered to be more suitable for higher energies, the quality of the agreement between the predictions and the experimental results is quite good. The radii show a similar behavior in their dependence on the isospin T_z as for lighter nuclei. In particular, the r_0^2 values increase linearly as a function of neutron-excess or isospin. The greater rate of increase as compared to model calculations in some systems suggests the existence of thin neutron skins. This result might be confirmed by further measurements and analysis that explore the difference between proton and neutron rms radii.

[1] I. Tanihata, H. Hamagaki, O. Hashimoto, Y. Shida, N. Yoshikawa, K. Sugimoto, O. Yamakawa, T. Kobayashi, and N. Takahashi, Phys. Rev. Lett. **55**, 2676 (1985).

[2] I. Tanihata, H. Hamagaki, O. Hashimoto, Y. Shida, O. Yamakawa, K. Sugimoto, T. Kobayashi, D. E. Greiner, N. Takahashi, and Y. Nojiri, Phys. Lett. **160B**, 380 (1985).

[3] I. Tanihata, T. Kobayashi, O. Yamakawa, S. Shimoura, K. Ekuni, K. Sugimoto, N. Takahashi, T. Shimoda, and H. Sato, Phys. Lett. B **206**, 592 (1988).

[4] T. Kobayashi, O. Yamakawa, K. Omata, K. Sigimoto, T. Shimoda, N. Takahashi, and T. Tanihata, Phys. Rev. Lett. **60**, 2599 (1988).

[5] D. Hirata, H. Toki, T. Watabe, I. Tanihata, and B. V. Carlson, Phys. Rev. C **44**, 1467 (1991).

[6] T. Minamisono, T. Ohtsubo, I. Minami, S. Fukuda, A. Kitagawa, M. Fukuda, K. Matsuta, Y. Nojiri, S. Takeda, and H. Kitagawa, Phys. Rev. Lett. **69**, 2058 (1992).

[7] W. Mittig, J. M. Chouvel, Zhan Wen Long, L. Bianchi, A. Cunsolo, B. Fernandez, A. Fotti, J. Gastebois, A. Gillibert, C. Gregoire, Y. Schutz, and C. Stephan, Phys. Rev. Lett. **59**, 1889 (1987).

[8] M. G. Saint-Laurent, R. Anne, D. Bazin, D. Guillemaud-Mueller, U. Jahnke, Jin Gen Ming, A. C. Mueller, J. F. Bruandet, F. Glaser, S. Kox, E. Liatard, Tsan Ung Chan, G. J. Costa, C. Heitz, Y. E-Masri, R. Hanappe, R. Bimbot, E. Arnold, and R. Neugart, Z. Phys. A **332**, 457 (1989).

[9] A. C. C. Villari, W. Mittig, E. Plagnol, Y. Schutz, M. Lewitowicz, L. Bianchi, B. Fernandez, J. Gastebois, A. Gillibert, C. Stephan, L. Tassan-Got, G. Audi, Wenlong Zhan, A. Cunsolo, A. Foti, A. Belezyorov, S. Lukyanov, and Y. Penionzhkevich, Phys. Lett. B **265**, 345 (1991).

[10] I. Licot, N. Added, N. Carlin, G. M. Crawley, S. Danczyk, J. Finck, D. Hirata, H. Laurent, D. J. Morrissey, M. M. de Moura, H. R. Schelin, J. Stasko, M. Steiner, A. A. P. Suaide, A. Szanto de Toledo, E. M. Szanto, M. Thoennessen, and J. A. Winger, Phys. Rev. C **56**, 250 (1997).

[11] *The Stopping Power and Ranges of Ions in Matter*, edited by J. F. Ziegler (Pergamon Press, New York, 1980), Vols. 2–6.

[12] S. Kox, A. Gamp, R. Cherkaoui, A. J. Cole, N. Longequeue, J. Menet, C. Perrin, and J. B. Viano, Nucl. Phys. **A420**, 162 (1984).

[13] S. Kox, A. Gamp, C. Perrin, J. Arvieux, R. Bertholet, J. F. Bruandet, M. Buenerd, R. Cherkaoui, A. J. Cole, Y. El-Masri, N. Longequeue, Phys. Rev. C **35**, 1678 (1987).

[14] Y. Ogawa, K. Yabana, and Y. Suzuki, Nucl. Phys. **A543**, 722 (1992).

[15] P. J. Karol, Phys. Rev. C **11**, 1203 (1975).

[16] Y. K. Gambhir, P. Ring, and A. Thimet, Ann. Phys. (N.Y.) **198**, 132 (1990).

[17] D. Hirata, K. Sumiyoshi, I. Tanihata, Y. Sugahara, T. Tachibana, and H. Toki, Nucl. Phys. **A616**, 438c (1997).

[18] A. Ozawa, T. Kobayashi, H. Sato, D. Hirata, I. Tanihata, O. Yamakawa, K. Omata, K. Sugimoto, D. Olson, W. Christie, and H. Wieman, Phys. Lett. B **334**, 18 (1994).

[19] H. Sato and Y. Okuhara, Phys. Rev. C **34**, 2171 (1986).

[20] T. Suzuki, H. Geissel, O. Bochkarev, L. Chulkov, M. Golovkov, D. Hirata, H. Irnich, Z. Janas, H. Keller, T. Kobayashi, G. Kraus, G. Munzenberg, S. Neumaier, F. Nickel, A. Ozawa, A. Piechaczek, E. Roeckl, W. Schwab, K. Summerer, K. Yoshida, and I. Tanihata, Phys. Rev. Lett. **75**, 3241 (1995).